Molecular Crystals and Liquid Crystals Science and Technology. Section A. Molecular Crystals and Liquid Crystals
Publication details, including instructions for authors and subscription information:
http://www.tandfonline.com/loi/gmcl19

The Static Nematic Director Field at Electrode Edges

Ch. Cramer [a], U. Kühnau [a], H. Schmiedel [a] & R. Stannarius [a]
[a] Fachbereich Physik, der Universität Leipzig, FRG

Version of record first published: 23 Sep 2006.

To cite this article: Ch. Cramer, U. Kühnau, H. Schmiedel & R. Stannarius (1994): The Static Nematic Director Field at Electrode Edges, Molecular Crystals and Liquid Crystals Science and Technology. Section A. Molecular Crystals and Liquid Crystals, 257:1, 99-112

To link to this article: http://dx.doi.org/10.1080/10587259408033767

Mol. Cryst. Liq. Cryst., 1994, Vol. 257, pp. 99–112
Reprints available directly from the publisher
Photocopying permitted by license only

The Static Nematic Director Field at Electrode Edges

CH. CRAMER, U. KÜHNAU, H. SCHMIEDEL and R. STANNARIUS

Fachbereich Physik der Universität Leipzig, FRG

(Received October 4, 1993; in final form January 7, 1994)

We have investigated planar LC cells with striped electrodes and two types of surface alignment of the director. Their optical properties are studied by means of polarizing microscopy, and a simple model is presented to determine the twist and tilt deformation of the director field. The optical patterns are simulated by computing the transmission function of the cell with model director deformations using the 4×4 matrix formalism. Depending on the director alignment at the surfaces, different types of inversion walls have been observed. They form structures of a characteristic geometry influencing the optical performance of LC devices. LC parameters may be calculated from the geometrical patterns of the observed defects. Any further attempt to calculate the exact static two-dimensionally (2D) deformed director fields in structured NLC cells ought to be checked by its consistency with the experimental effects reported here.

Keywords: Nematics, director field, surface alignment, inversion walls, LCD

1. INTRODUCTION

The static properties of planar homogeneously deformed nematic liquid crystal (NLC) layers are well investigated. Their optical behavior can be calculated using the Berreman's 4×4 method. In modern display technique, however, structured electrodes of ever decreasing dimensions are used. The electrode structures become comparable to the cell thickness and the occurring inhomogeneities of the electric field near the electrode edges cannot be neglected any longer. In addition to the field inhomogeneities, inversion walls appear which influence the optical properties of the LC device.

Meanwhile, attempts have been made to build flexible lenses based on LC cells with special electrode geometries, which make use of the optical behavior of two-dimensional deformed NLC layers.[1,2]

Several works have been published dealing with the theoretical description of static 2D- and 3D-inhomogeneously deformed director fields.[3,7] Most of these publications consider a pure tilt deformation only. In opposition to these assumptions, our experimental results give clear evidence of an additional twist deformation.

In a previous paper [8] we have reported a first method for the study of the static director distribution by recording the optical transmission. In this paper, another method is presented which allows us to deduce the deformation of the director field using a simple model. Furthermore, a model is presented which describes the voltage dependence of the orientation and the width of the inversion walls of the twist-bend

type, arising in the case of a surface director orientation perpendicular to the electrode strips as a consequence of the field inhomogeneities at the edges. In a subsequent article, we will report our investigations of the dynamical behavior of the LC cells when an electric fields is switched on or off.

2. EXPERIMENTAL

We have investigated NLC cells with two different types of surface orientation of the director. In Figure 1 the principal geometry of both types is shown as a projection onto the xy- and the xz-plane, respectively. The angles $\Theta(x, y, z)$ and $\varphi(x, y, z)$ are the local tilt and twist angles of the director field. The dimensions of the cell are approximately 20×10 mm. The ITO-electrodes are manufactured as a plane and unstructured one at the lower glass plate and a set of 19 parallel strips at the upper glass plate. Since the strips are long (≈ 10 mm) compared to the cell thickness ($\approx 7\,\mu$m) and the electrode width, the cell geometry can be considered as two-dimensional. Two sets of cells have been available with 100 μm and 16 μm electrode width, respectively. The electrodes are separated by gaps of equal width.

The planar orientation of the director at the surfaces has been achieved by oblique evaporation of SiO_x ($1 < x < 2$) [10]. The pretilt is lower than 1°. The cells exhibit

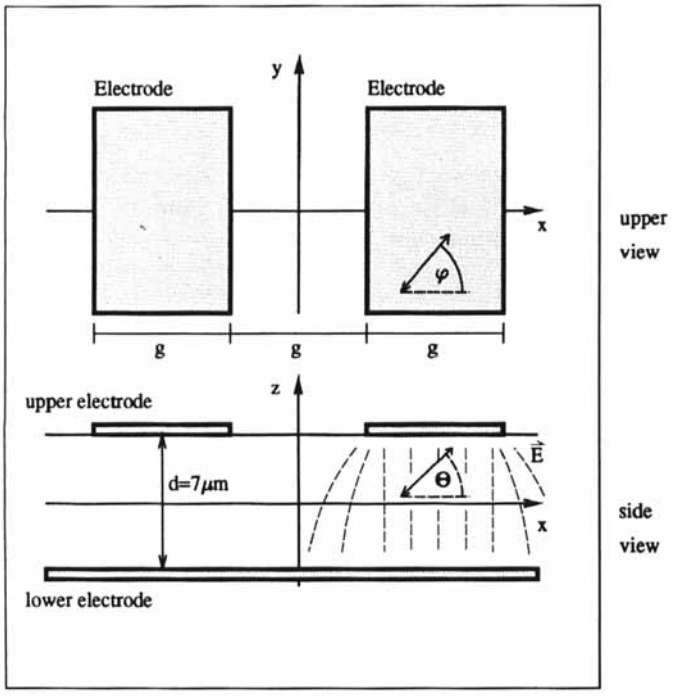

FIGURE 1 Upper and side view of the sample with the definition of the tilt (Θ) and the twist (φ) angles of the director field, the widths of electrode and gap (g), and the cell thickness (d).

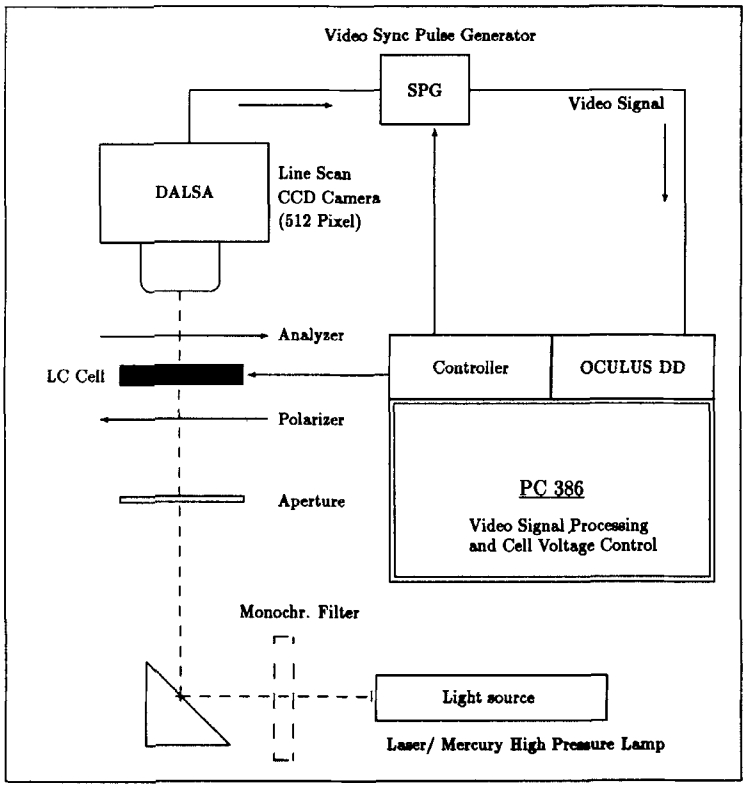

FIGURE 2 Schematic view of the experimental setup; The light path is given as a dashed line.

strong anchoring and no intrinsic twist. The two investigated types of surface alignment with respect to the electrode direction are the following:

- director alignment perpendicular to the strips, $\vec{n}(0) = \vec{n}(d) = (1,0,0)$ (case $n_\perp$)
- director alignment parallel to the strips, $\vec{n}(0) = \vec{n}(d) = (0,1,0)$ (case $n_\parallel$)

The cells have been filled with the pure nematic substance PCH5 (Merck). The viscoelastic, dielectrical and optical data of this substance are well known [11, 12]. In good agreement with the theoretical data, the Fréedericksz threshold was determined to be 0.88 V at $T = 30.3°C$. The samples were thermally stabilized and placed into a polarizing microscope. The experimental setup is given in Figure 2. As a light source, a laser and a mercury high pressure lamp were used alternatively. For a first, rough investigation, we have placed the sample between crossed polarizers with the strips in the diagonal, illuminating it with white light, to get a qualitative estimation of the director distribution across the electrode.

In another experiment, the optical transmission of monochromatic light has been recorded as a function of the orientation of the polarizers with respect to the electrode direction, voltage and temperature being kept constant. The interference between ordinary and extraordinary light was recorded by a DALSA CCD line scan camera

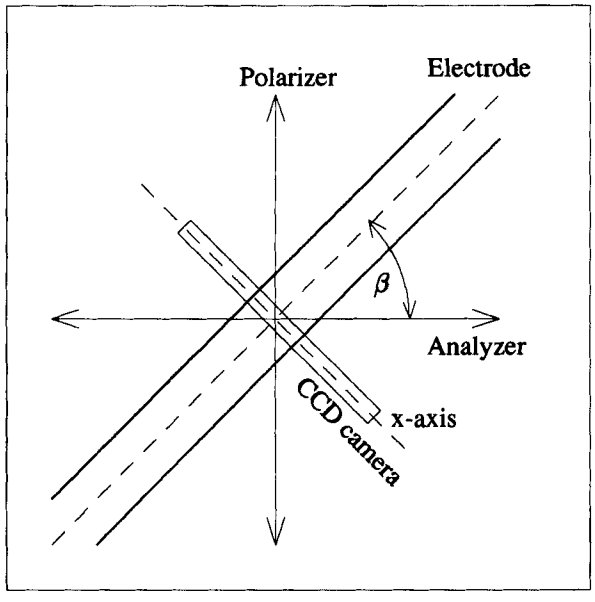

FIGURE 3 Orientation of the electrodes with respect to the polarizers and the CCD camera.

with 512 pixel resolution oriented perpendicular to the strip direction (see Figure 3). Such, the camera delivers a cross section profile of the transmitted light intensity perpendicular to the electrode. The same information can be deduced from images recorded by a matrix CCD camera if a quartz wedge is inserted into the light path. The wedge has to be placed between crossed polarizers with its main axis parallel to the x-direction. The sample is illuminated with monochromatic light. Due to the additional linearly increasing phase retardation of the quartz wedge, the phase retardation in the liquid crystal layer is transformed into a shift of the interference pattern in y-direction.

In the case of perpendicular oriented LC cells ($n_\perp$), the information obtained with the line scan camera is not sufficient. The zig-zag twist-bend inversion walls [8], appearing after switching the electrodes into the ON state, have a three-dimensional structure. Any cross section through the sample along the x-axis intersects these zig-zag walls at a different position. For the image recording in that case, a matrix CCD camera was used.

3. THEORY

In this section, the fundamental optics and models for the interpretation of the recorded pictures are discussed. As seen in Figure 4, the cross section of the electrodes can be divided into regions where the director orientation is almost uniform along x, and into regions in the vicinity of walls which are small compared to the electrode sizes. In the regions outside the walls, the director field can be described by a set of tilt and twist

angles Θ and Φ which may be derived from the optical transmission function. In contrast, the walls are characterized by a large deformation of the director field, diffraction effects influence the microscopic picture. The director field can be resolved spatially only qualitatively. Thus, we have to introduce additional assumptions on the director field in the wall, and we can only determine global features of these walls like the wall thickness and orientation.

In the first part, we restrict ourselves to the areas far from the walls. The director field in the vicinity of the walls is considered in the second part.

3.1. Analysis of the Director Field far from the Walls

For crossed polarizers in orientation $\beta = 45°$ to the director, in the undistorted cell the phase retardation Δ_L between the ordinary and extraordinary transmitted light waves is $\Delta_L(\Theta = 0) = \Delta_{L0} = 2\pi \cdot \Delta n \cdot d/\lambda = 9.420$ for $\lambda = 544\,\text{nm}$ and $T = 30°\text{C}$, where $\Delta n = n_e - n_o = 0.1165$ is the corresponding birefringence of PCH5 at 30°C. This gives a constant intensity of the transmitted light $I_{A0} = I_0 \sin^2(2\beta) \sin^2(\Delta_{L0}/2) \approx I_0 \sin^2(2\beta)$ almost exactly at the 2nd interference maximum. Including a pure tilt deformation of the

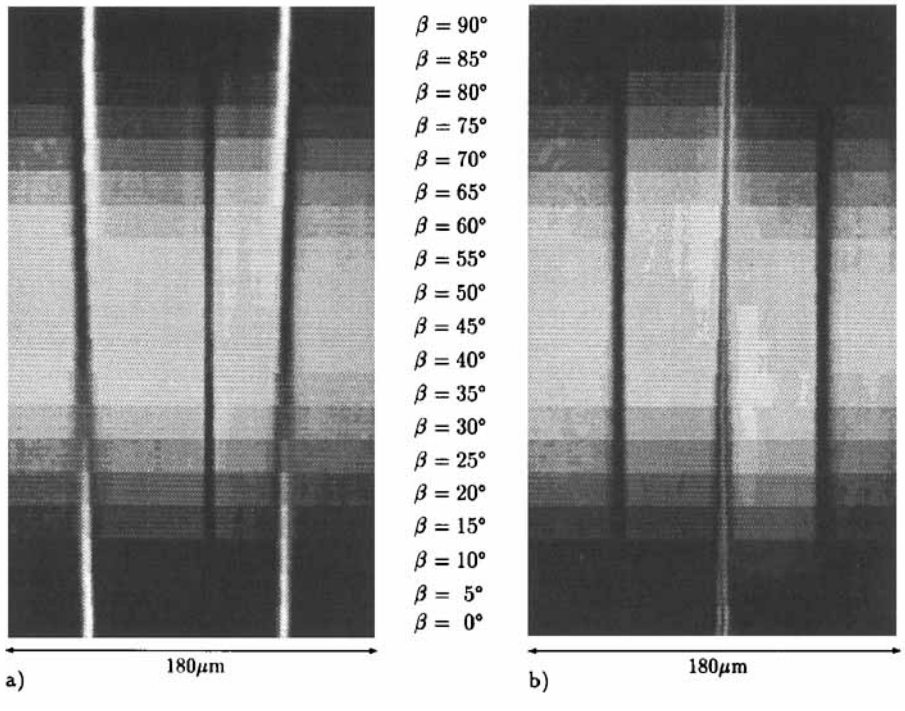

FIGURE 4 Transmitted light intensity profiles across one electrode strip (100 μm) for the $n_\parallel$ cell (**a**) and the $n_\perp$ cell (**b**). The boundary regions are seen as vertical twisted (a) or dark (b) bands. Walls within the electrodes appear as vertical dark or twisted bright and dark bands. In the dark bands, twist of the director along z is absent whereas the twisted structures correspond to complex tilt and twist deformations of the director field (see text).

director field, n_e has to be replaced by

$$n_{eff}(x) = 1/d \int_0^d \frac{n_e n_0}{\sqrt{n_e^2 \sin^2(\Theta(x,z)) + n_o^2 \cos^2(\Theta(x,z))}} dz \tag{1}$$

The phase retardation is decreasing with increasing director deformation, passing an interference minimum into the first interference maximum at $\Delta_L = \pi$ and finally reaching zero for a director field which is completely switched parallel to $\vec{E}$ at high voltages ($\Theta \equiv \pi/2$). In Figure 4, transmission profiles for different β (vertical axis) are shown where the electric field at the electrode was chosen such that the intensity was at the first interference maximum in the electrode area. In the case of striped electrodes, we expect an inhomogeneously deformed director field not only normal to the cell but also across the electrode structure. With a two-dimensionally inhomogeneous tilt ($\Theta(x,z) \neq 0$), and twist ($\varphi(x,z) \neq 0$) of the director field, the calculation of the optical properties becomes very complicated. First, the computation of the director field requires the self-consistent solution of a set of differential equations for the director tilt $\Theta(x,z)$ and twist $\varphi(x,z)$ and for the electric field $\vec{E}(x,z)$. Second, if the optical inhomogeneity of the medium becomes comparable to the light wavelength λ, one cannot longer use geometrical optics, nor even the Berreman's 4×4 matrix method to determine the optical transmission of the sample from the known director profile. The exact calculation of the optical properties requires the complete solution of the Maxwell equations for light propagation in the sample.

We can, however, facilitate the description of the experiment by introducing the assumption that the optical inhomogeneity of the medium in x direction is small, i.e., the refractive indices are considered constant at distances compared to the light wavelength.

This approximation is justified by the large size of the electrode stripes compared to λ. Deviations may occur only very close to the electrode edges, they show up as focussing effects. However, it can be seen from the experimental intensity profiles that such effects are small and can be neglected within the spatial resolution of the camera of approximately 0.7 μm. Besides, the thickness of the investigated cell is small enough (7 μm) to justify the application of locally geometrical optics. Furthermore, as the optical transmission data are not sufficient to provide complete information on the director field in the cell, we introduce model functions $\Theta(x,z)$ and $\varphi(x,z)$. Outside the walls and far from the electrode edges, these functions coincide with functions $\Theta = \Theta_{1D}(z)$ and $\varphi = 0, 90°$ resp., which minimize the free energy functional for the one-dimensionally deformed nematic [9].

The model function $\varphi(x,z) = \varphi_m(x) \cdot \sin(\pi z/d)$ with φ_m being the twist angle in the middle of the cell, may differ somewhat from the exact solution of the two-dimensional director field at the electrode edges but the principle quantitative changes with φ_m as well as the effects observed experimentally are correctly reproduced. It should be noted that in the following we will commonly refer to Θ as the tilt angle and φ as the twist angle which is meant with respect to the surface director. Of course, a twist deformation along x may be related to the angle Θ as well, and a variation of φ along x will lead to splay-bend energy terms.

Using these simplifications, the optical transmission pattern can be calculated as a function of the x-coordinate making use of the Berreman's method [13] which is valid

for 1D-inhomogeneously deformed LC layers. The transmitted light intensity for normal incidence is computed separately at each position x. This implies that light passes the cell without deflection. For the 7 μm cell, this is a good approximation as will be shown by comparison with the experiment. Recording the transmitted intensity at several orientations β (rotating the crossed polarizers with respect to the electrode axis) at constant cell temperature and electric field, one obtains a β-dependent function which provides information on the director tilt and twist deformation in the cell in a rather complicated way. By fitting the calculated transmission functions to the experimental patterns we determine the director field.

3.2. Inversion Walls

In the two cases of director surface alignment, different types of inversion walls are observed. In the $n_{\parallel}$ case, twist inversion walls arise due to the energetical equivalence of positive and negative tilt angles. In most cases, only one wall occurs, but up to seven have been observed within the width of the electrode. These walls vanish after a limited period of time due to the director relaxation into one direction. A shift of the walls along the x-axis does not require elastic energy, thus, they may shift to the electrode edges and finally disappear.

In the perpendicularly oriented LC cells, the director starts to tilt with opposite sense of rotation on both electrode edges, due to the inhomogeneous electric field. One stable twist-bend wall is necessarily generated, forming a zig-zag line near the middle of the electrode (see Figure 5) and separating regions of opposite tilt angle. These zig-zag walls exhibit a characteristic inclination angle α formed by the linear parts of the wall

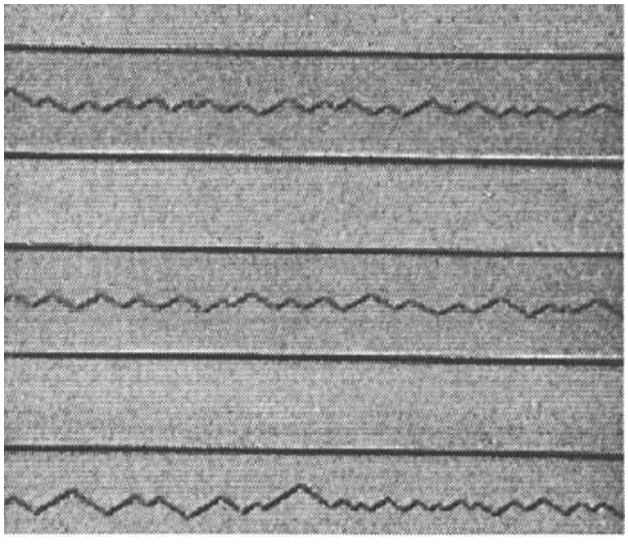

FIGURE 5 Top view of a LC cell with striped electrodes between crossed polarizers (case $n_{\perp}$, 7 μm cell thickness, 100 μm electrode width, PCH5, $T = 28°$); Three electrodes are shown in the picture. The small zig-zag lines in the electrode area are the twist-bend walls. They separate regions with opposite tilt angles. $U = 3.0$ V.

with the electrode axis, and a typical width. The angle α depends upon voltage, temperature and material constants, but not upon the electrode width. Since the angle is well reproducible, it allows the determination of the ratio of elastic constants as shown below. Such inversion walls in dielectrically deformed LC layers with planar boundary conditions were investigated earlier by Stieb *et al.* [14]. In the case of strip shaped electrodes the two regions of opposite tilt at both electrode edges produce a strong deformation in the middle of the electrode. Because of the smaller twist elastic constant K_2 compared to K_1 and K_3, the splay and bend deformation is partially replaced by a twist deformation with the result of a decrease of the free energy of the wall [15]. This is achieved by a change of the wall orientation with respect to the surface director. Applying these ideas to interpret the results obtained by investigation of the samples between crossed polarizes in 45° position when illuminated with white light, a quite simple model for the director deformation in the wall has been developed which allows the calculations of the inclination angle α and the wall thickness d_w in dependence on voltage and temperature.

The calculations are based on the minimization of the free energy per length of the electrode strip. Since the width of the electrodes is large compared to the thickness of the wall, it is assumed that the deformation of the director field and of the electric field outside the inversion walls is the same as in a one-dimensionally deformed LC layer. As a second assumption, the width of the wall and of the corresponding deformation of the electric field are considered to be of equal size. To describe the director distribution inside the walls, a model ansatz for the tilt and twist angle is introduced, making use of the results of the observations by polarizing microscopy:

$$\Theta(\xi, z) = \Theta_0(z)\,\vartheta(\xi) \tag{2}$$

$$\varphi(\xi, z) = \varphi_1 \cdot \sin\left(\frac{\pi\xi}{d_w}\right) \cdot \sin\left(\frac{\pi z}{d}\right)$$

where ξ is the coordinate perpendicular to the local orientation of the twist-bend wall, $\Theta_0(z)$ is the solution for the tilt angle outside the wall as found by solving the Euler–Lagrange equations for the 1D-inhomogeneously deformed LC layer (see Figure 6). As boundary conditions, $\vartheta(\xi)$ has to satisfy the relations $\vartheta(0) = -1$, $\vartheta(d_w) = 1$ and $\vartheta(d_w/2) = 0$ which provide continuity of the tilt angle at both sides of the wall. φ_1 is a measure for the non-zero twist in the wall. Finally, the ansatz for the electric potential has to be symmetrical with respect to the middle of the wall and has to change continuously into the potential distribution outside the twist-bend walls which can be determined from 1D director field calculations [9].

w_{el}^0 and w_{el}^{in} being the densities of the electrical energy outside and inside the walls, resp., and w_d^0 and w_d^{in} being the densities of the energy of elastic deformation, one obtains the following functional for the free energy per unit length:

$$F(d_w, \varphi_1, \vartheta, \alpha) = 4 \int_0^{d_w/2} d\xi \int_0^{d/2} dz (w_d^{in}(\xi, z) - w_{el}^{in}(\xi, z)) - d_w \cdot w^0 \tag{3}$$

$$w^0 = w_d^0 - w_{el}^0$$

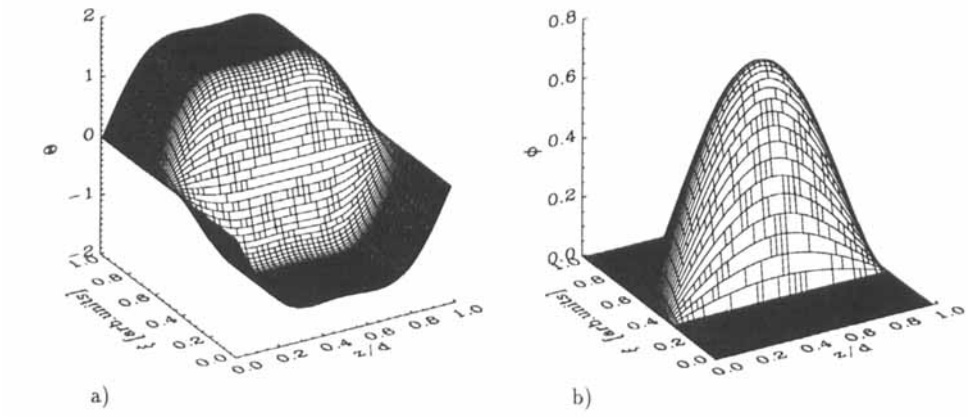

FIGURE 6 Three-dimensional representation of the director deformation angles $\Theta(\xi, z)$ (**a**) and $\varphi\ (\xi, z)$ (**b**) used in the simulation of the twist-bend wall in the centre of the $n_\perp$ electrode.

constant contributions being neglected. The integration is over the wall area where a 1D-deformed director field of opposite tilt is assumed on both sides of the wall. The minimum of the functional is found by variation of the free parameters α, d_w, φ_1 and the first 3 Fourier coefficients of $\vartheta(\xi)$.

On the basis of this minimization, one finds a model of the director distribution which can be used to calculate the optical behavior of the layer. Using the same assumptions as in Section 3.1, one can determine the intensity of the transmitted light in dependence upon the angle β. The transmission function at each point x for normal incidence is calculated separately by application of the Berreman formalism. This simulated intensity profile is compared with the recorded images of the walls.

In Figure 7a, we show the calculated transmission of light for a twist-bend wall as depicted in Figure 6. The horizontal axis gives the spatial coordinate x perpendicular to the electrode strips, the vertical coordinate corresponds to the rotation of β as in Figure 4b. The tilt angle is equal to the solution Θ_{1D} of the one-dimensional non-twisted director field at both sides of the wall, it changes its sign across the wall. The twist angle φ is zero at both sides of the wall and maximum in its middle. The coincidence with the pattern observed in the middle of the $n_\perp$ type strip is clearly seen.

Figure 7b shows the optical pattern related to the functions

$$\Theta(x, z) = \Theta_{1D}(z) * \sin^2(\pi x/2d_t) \tag{4}$$

$$\varphi(x, z) = \varphi_m * \sin(\pi z/d) * \sin(\pi x/d_t)$$

with the dimension of the transition region d_t and $\varphi_m = 1.05$. This deformation corresponds to the director field at the electrode boundaries in the $n_\parallel$ cell. The good agreement with the experiment is seen from a comparison with Figure 4a. The tilt is zero at $x = 0$ and Θ_{1D} at the boundary $x = d_t$. The twist angle φ is zero at both sides of the transition region and maximum in its centre.

In Figure 7c, the optical transmission for the pure Θ-deformation is depicted ($\phi \equiv 0$ or $\varphi \equiv 90°$). One can easily see the coincidence with the edges of the $n_\perp$. The

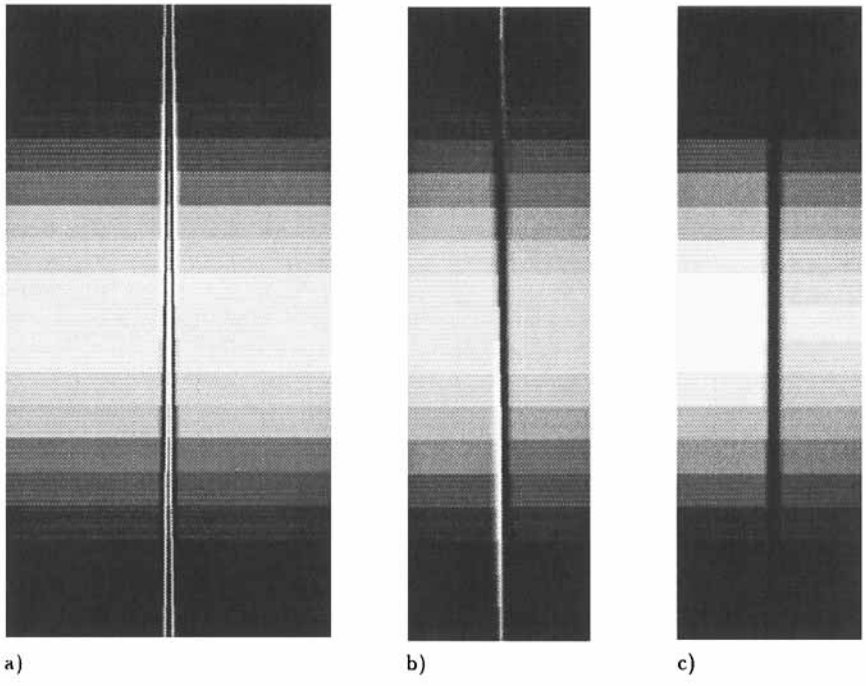

FIGURE 7 Simulation of the optical transmission profile along x for different β; (**a**) calculated transmission of light for a twist-bend wall as depicted in Figure 6; The horizontal axis is along x and the vertical coordinate corresponds to β as in Figure 4b. The image corresponds to the experimental pattern in the middle of the $n_\perp$ type electrode. (**b**) calculated optical pattern for the boundary region in the $n_\parallel$ cell; (**c**) simulated optical transmission for the pure Θ-deformation in the $n_\perp$ cell.

characteristic feature is a vertical black line where the director is tilted such that the integral of n_{eff} according to Equation [1] gives an interference minimum ($\Delta_L = 2\pi$) irrespective of β. In both cases, the twist angle can be neglected.

4. RESULTS

An new method of polarizing microscopy is presented which allows the determination of director distributions in two-dimensional inhomogeneously deformed nematic layers. The local application of the 4×4 matrix formalism for normal light incidence proved to be successful in the description of the optical transmission properties of the cells even with the observed 2D deformed director fields. We have applied it to study thin cells with complex director deformations induced by structured electrodes. If the transmission of the cells is recorded without polarizers, one finds no change in the intensity after switching the electrode voltage. This proves that we can exclude focussing effects near the electrode edges and assume a normal transition of the incident light through the cells. The observed transmission patterns are pure interference effects between the ordinary and extraordinary light waves in the sample.

For a discussion of the general effects of a director field near the edge of an electrode, it is necessary to understand that the orientation of the director alignment at the surface with respect to the edge is of basic importance for the structure of the deformation. Planar cells with small electrode strips parallel and perpendicular to the alignment direction have been investigated as simple model systems.

The Figures 4a, b show sections of the optical transmission patterns across an electrode strip for the $n_\parallel$ and $n_\perp$ geometry, resp. The width of the pictures in x direction corresponds to 180 μm. One electrode strip of 100 μm is visible in the centre of each figure. The transmission patterns recorded in the figures correspond to the static director field at constant voltage U = 2.55 V ($U_c = 0.88$ V). Crossed polarizers have been rotated by $\beta = n \cdot 5°$ ($n = 0, 1, \ldots, 18$ top to bottom in the figures) with respect to the direction of the electrode strip.

We will first discuss the case $n_\parallel$ with the electrode edge parallel to $\vec{n}_0$. In the case of parallel oriented cells, the electric stray field at the electrode boundary has a component perpendicular to the tilt plane (e.g., [3, 5]). The director twists out of the plane formed by surface alignment $\vec{n}_0$ and cell normal, in addition to the tilt deformation. The maximum twist of approximately $\varphi_m = 1.05$ is found along the electrode edges. Far from the electrode boundary inside and outside the electrode area, the twist angle φ is zero. Figure 7b gives a corresponding simulated transmission pattern. The approximate width of the transition region of 14 μm is comparable to the cell thickness. Tilt angles Θ and $-\Theta$ are energetically equivalent, therefore the director may initially tilt in both rotation senses with equal probability. The optical transmission is independent of the sign of tilt.

In the 100 μm striped electrode, domains of opposite tilt may appear. They are separated by twist walls which extend along the electrode parallel to its edge. The number of twist walls observed after switching the cell on varies unpredictably for each individual experiment, because thermal director fluctuations initiate the switching process of the cell and one or more domains are formed. Usually one such wall was observed, but there may be multiple walls or even none. These twist walls may be described approximately by a function $\Theta(x, z) = \Theta_{1D}(z) * \cos(\pi x / d_w)$ for $0 < x < d_w$. This corresponds to a change of the sign of Θ across a wall of thickness d_w, with the boundary conditions $\pm\Theta_{1D}(z)$ at both sides being the solution of the plane cell without electrode structure. If multiple walls are observed, they have alternating signs in Θ. Because of comparably small elastic constant K_2, the thickness of the twist walls is very small. Therefore, they could not be resolved spatially.

The twist walls are instable because in the electrode plane, they may shift in x direction without a change of the elastic deformation energy. Two adjacent twist walls may annihilate each other. Usually the walls move towards the electrode boundaries where they disappear.

In the case of electrode edges perpendicular to the surface alignment, the initial director orientation coincides with the x-direction and therefore, the director tilts in the xz-plane formed by the $\vec{n}_0$ and the electric stray field. No additional twist occurs at the electrode edge. The optical appearance of the director field at the edge is therefore well described by the model used in the calculation of Figure 7c where $\Theta(x, z) = \Theta_{1D}(z) * \sin^2(\pi x / 2d_t)$. Θ is zero at the outer boundary of the transition region and equal to the 1D solution at the inner boundary. The twist angle φ is zero. The width of the transition

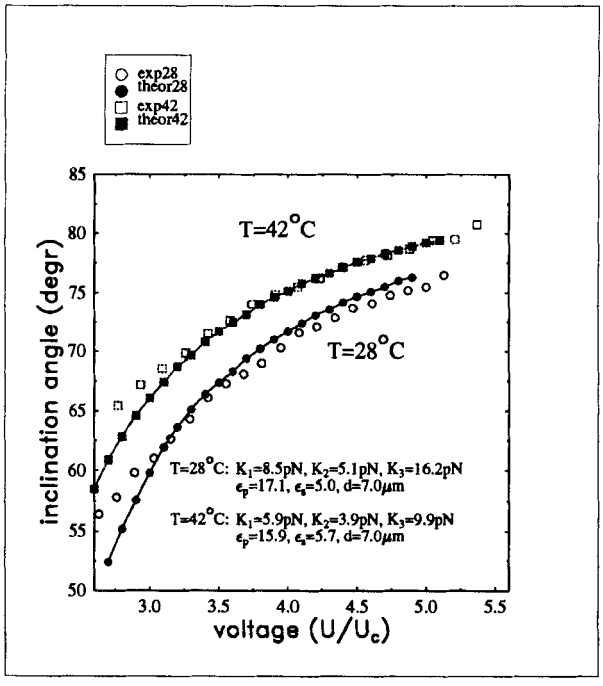

FIGURE 8 Experimental (markers) and theoretical (line) values of the inclination angle α of the twist-bend wall for $T = 28°C$ and $T = 42°C$ versus the reduced voltage U/U_c(U_c... Fréedericksz thresold); sample parameters are given in the figure.

region at the electrode edge is approximately 13 μm which again is of the order of the cell thickness.

In the striped electrode, always exactly one splay-bend wall appears in the middle of the electrode strip after switching to voltages above the Fréedericksz threshold. Such types of walls are very stable as they cannot shift towards the electrode edge where the oblique electric stray field pins the opposite tilt of the director. However, changing locally its orientation with respect to n_0, the wall may partially replace splay-bend deformation by twist, on the cost of an elongation of the wall. Thus these walls form a characteristic zig-zag geometry depending on the applied voltage, the cell thickness, and the material constants. The zig-zag angle α can be influenced reproducibly by alternating the applied voltage U at the cell. Using the variation principle to minimize the free energy with simple model expressions for tilt and twist within the wall, we can describe the director field satisfactorily and the ratio of elastic constants may be determined from $\alpha(U)$. In Figure 8, the experimental and fitted values of the inclination angle vs. voltage for the given set of parameters can be seen. The curves for two different temperatures are given. Figure 4b shows the characteristic optical appearance of the wall. It is well reproduced in the simulation of Figure 7a where a director deformation profile according to our model has been assumed. Zig-zag walls of a comparable appearance have been found already by Haas in his optical study of the director field of a pixel electrode [3].

If the transmission pattern in Figure 4b is studied thoroughly at both sides of the central twist-bend wall, one can see that the transmitted intensity function $I(\beta)$ has slightly changed its phase in β, compared to the $\sin^2(2\beta)$ dependence of the undeformed director outside the electrodes. For $\varphi \equiv 0$, it should be strictly proportional to $\sin^2(2\beta)$ with an amplitude proportional to $\sin^2(\Delta_L/2)$ (planar director distribution in the xz plane). This sine dependence is actually shifted by approximately 5° into opposite directions on the β axis at both sides of the central wall. This means that the director is twisted out of plane all over the electrode, in a rough approximation by an average angle of $\varphi = 5°$. That is, the influence of the central twist-bend wall reaches far outside the wall, up to distances comparable to the half electrode width. In the calculations, we have neglected this effect which should be of minor influence on the structure of the wall itself.

5. CONCLUSIONS

The experimental effects described in this paper should give an impact to theoretical studies of two and three-dimensional director deformations. Further attempts of an exact calculation of the director field in such systems should be checked by their consistency with the results reported here.

In arbitrarily shaped electrodes, edges parallel, perpendicular and oblique to the surface director alignment $\vec{n}_0$ may be present simultaneously. As we have shown, edge effects extend over regions comparable to the cell thickness. As long as the electrode size is larger than the cell thickness, one can consider the individual edges separately and assume a director field similar to that of the unstructured homogeneous Fréedericksz transition inside the electrode area far from the edges. Then, a twist angle φ will be induced at all electrode edges except those perpendicular to $\vec{n}_0$. At the other electrode boundaries, the $\vec{E}$ field has a component out of the $\vec{n}_0$-z-plane which induced out-of plane twist. Thus, we expect a smaller but non-zero twist angle also along electrode edges oblique to $\vec{n}_0$.

The appearance of zig-zag twist-bend walls is also not restricted to strip shaped electrodes. Such walls have been reported for square electrode pixels by Haas [3], too. In his observations, the zig-zag wall appeared close to one edge of the electrode because of the high pretilt of surface director in the cell (2°). He used a different surface preparation method. Obviously, those walls should appear with other electrode shapes, too. The angle α between the surface director and the local wall segments depends upon liquid crystal properties and the electric field, so we expect it to be independent of the actual electrode shape, whereas the position of the wall as well as their general orientation (determined by the relative lengths of the zig-zag segments) should be adapted to the electrode shape.

In addition in the work of Haas, other effects are discussed, which are observed in TN cells (director alignment at the upper and lower glass surfaces twisted by 90° with respect to each other).

Finally we consider the case where not only the upper but also the lower electrode is structured. If the electrode edges of the upper and lower electrode do not coincide, like in two perpendicular stripe pattern at the upper and lower glass plate, the edges may be

treated similar to the case of a structured electrode and an unstructured counter-electrode. If both electrodes have the same extension, and their edges coincide, the electric stray field is different. Because of the symmetry in z (the coordinate normal to the cell), the electric field vector $\vec{E}$ will be normal to the cell plane in the middle of the cell, the component of $\vec{E}$ perpendicular to the electrode edge will be much smaller and has its maximum in the vicinity of the glass plates, with opposite declination at both glass surfaces. Therefore, no preferred tilt direction exists and we do not expect any of the effects observed at our $n_\perp$ stripes. At the $n_\parallel$ type electrode edges, the effect of an induced twist angle may still exist but should be orders of magnitude smaller. The conclusions made in this last paragraph have been drawn on the basis of our experimental investigations on the simple stripe systems. They are left to be confirmed by future experimental investigations.

Acknowledgement

The authors are indebted to V. Skokow for his technical support in the installation of the experimental setup. This work was supported by the Deutsche Forschungsgemeinschaft under grant Schm 902/2-1.

References

1. T. Nose and S. Sato, *Liq. Cryst.*, **5**, 1425 (1991); T. Nose, S. Masuda and S. Sato, *Mol. Cryst. Liq. Cryst.*, **199**, 27 (1991); T. Nose, S. Masuda and S. Sato, *Jpn. J. Appl. Phys.*, **31**, 1643 (1992).
2. S.T. Kowel, D. S. Cleverly and P. G. Kornreich, *Appl. Optics.*, **23**, 278 (1984); S. T. Kowel, P.G. Kornreich and A. Nouhi, *Appl. Optics.*, **23**, 2774 (1984).
3. G. Haas, H. Wöhler, M. Fritsch and D. A. Mlynski, *Mol. Cryst. Liq. Cryst.*, **198**, 15 (1991); G. Haas, Freiburger Arbeitstagung Flüssigkristalle 1991 Proceedings P24.
4. V. Chigrinov, *Mol. Cryst. Liq. Cryst.*, **71**, 179 (1990).
5. M. Schmidt, *Mol. Cryst. Liq. Cryst.*, **65**, 206 (1991).
6. S. Dickmann, O. Cossalter, J. Eschler and D. A. Mlynski, Freiburger Arbeitstagung Flüssigkristalle 1992 Proceedings P04.
7. F. Schwabe, P. M. Knoll, S. Dickmann, J. Eschler and D. A. Mlynski, Poster at the 13th European. *Liq. Cryst. Conf. Films.*, 1993.
8. H. Schmiedel, Ch. Cramer, R. Stannarius, K. Eidner and M. Grigutsch, *Liq. Cryst.*, **14**, 1935 (1993).
9. H. J. Deuling, *Mol. Cryst. Liq. Cryst.*, **19**, 123 (1972).
10. J. Cognard, *Mol. Cryst. Liq. Cryst.*, Suppl. Ser. **1**, 1 (1982).
11. U. Finkenzeller, T. Geelhaar, G. Weber and L. Pohl, *Liq. Cryst.*, **5**, 313 (1989).
12. A. Scharkowski, Dissertation Leipzig 1990.
13. D. W. Berreman, *J. Opt. Soc. Am.*, **62**, 502 (1972).
14. A. Stieb, G. Baur and G. Meier, *Ber. Bunsenges.* **78**, 899 (1979).
15. F. Brochard, *J. de Physique*, **33**, 607 (1972).